PCCP

PAPER

View Article Online
View Journal | View Issue

Cite this: *Phys. Chem. Chem. Phys.*, 2016, **18**, 16766

Imaging fluorescence correlation spectroscopy studies of dye diffusion in self-assembled organic nanotubes†

Hao Xu,[a] Shinobu Nagasaka,[a] Naohiro Kameta,[b] Mitsutoshi Masuda,[b] Takashi Ito*[a] and Daniel A. Higgins*[a]

Received 6th May 2016,
Accepted 27th May 2016

DOI: 10.1039/c6cp03069f

www.rsc.org/pccp

The rate and mechanism of diffusion by anionic sulforhodamine B (SRB) dye molecules within organic nanotubes self-assembled from bolaamphiphile surfactants were investigated by imaging fluorescence correlation spectroscopy (imaging-FCS). The inner and outer surfaces of the nanotubes are terminated with amine and glucose groups, respectively; the former allow for pH-dependent manipulation of nanotube surface charge while the latter enhance their biocompatibility. Wide-field fluorescence video microscopy was used to locate and image dye-doped nanotubes dispersed on a glass surface. Imaging-FCS was then used to spatially resolve the SRB transport dynamics. Mobilization of the dye molecules was achieved by immersion of the nanotubes in buffer solution. Experiments were performed in pH 6.4, 7.4 and 8.4 buffers, at ionic strengths ranging from 1.73 mM to 520 mM. The results show that coulombic interactions between cationic ammonium ions on the inner nanotube surface and the anionic SRB molecules play a critical role in governing mass transport of the dye. The apparent dye diffusion coefficient, *D*, was found to generally increase with increasing ionic strength and with increasing pH. The *D* values obtained were found to be invariant along the nanotube length. Mass transport of the SRB molecules within the nanotubes is concluded to occur by a desorption-mediated Fickian diffusion mechanism in which dye motion is slowed by its coulombic interactions with the inner surfaces of the nanotubes. The results of these studies afford information essential to the use of organic nanotubes in controlled drug release applications.

Introduction

Self-assembled organic nanotubes have been prepared from a variety of materials, including proteins, peptides, synthetic and natural lipids, and synthetic organic amphiphiles.[1–3] Synthetic nanotubes have attracted particular interest because they afford access to tailor-made materials with hydrophobic, hydrophilic and/or biocompatible outer surfaces, uniform tubular morphologies and internal nanospaces of controllable dimensions and surface chemistries. These attributes make them suitable for use in a wide variety of applications, including as nanopipettes,[4] nanocontainers for biomacromolecules[5] and as vehicles for drug delivery.[6–8]

An unique subset of synthetic organic nanotubes are those derived from bolaamphiphile surfactants.[5] Unlike many surfactant assemblies, bolaamphiphile-based materials afford nanotubes with differently functionalized (and functionalizable)[9] hydrophilic internal and external surfaces that can be used to encapsulate and transport water-soluble molecules into aqueous biological environments. Kameta and coworkers have recently synthesized bolaamphiphile-based nanotubes incorporating amine groups on their internal surfaces and sugars on their external surfaces.[5] The sugars improve nanotube biocompatibility, while the amine terminated internal surfaces provide the means to load and immobilize molecules within the nanotubes, as well as allowing for them to be released in response to some stimulus.[10,11] Release of encapsulated molecules into the surrounding medium relies upon, among other factors, their diffusion within the nanotubes.[12,13] An in-depth understanding of mass transport rates and mechanisms within organic nanotubes is therefore critical to the development of materials for controlled release applications.

Molecular diffusion within nanoscale pores and microdomains can be explored by a number of different optical imaging and spectroscopic methods, including single molecule tracking (SMT),[14,15] fluorescence recovery after photobleaching (FRAP),[16–18] fluorescence resonance energy transfer (FRET) imaging,[9] confocal fluorescence correlation spectroscopy (FCS)[18] and imaging-FCS.[19] SMT has been used previously to investigate the effects of surfactant

[a] *Department of Chemistry, Kansas State University, Manhattan, KS 66506-0401, USA. E-mail: ito@ksu.edu, higgins@ksu.edu*
[b] *Research Institute for Sustainable Chemistry, Department of Materials and Chemistry, National Institute of Advanced Industrial Science and Technology (AIST), Tsukuba Central 5, 1-1-1 Higashi, Tsukuba, Ibaraki 305-8565, Japan*

† Electronic supplementary information (ESI) available: Supporting information and a representative fluorescence video. See DOI: 10.1039/c6cp03069f

nanostructures on molecular diffusion within one dimensional (1D) lyotropic liquid crystal mesophases.[20] However, SMT is difficult to implement in the characterization of single organic nanotubes, because of the low dye concentrations required. FRAP is a common ensemble method that has recently been used to probe diffusion in the 1D poly(ethylene oxide) microdomains of phase separated poly-(ethylene oxide)-polystyrene block copolymer films.[16] Unfortunately, FRAP is best suited to investigations of diffusion over long distances (*i.e.*, >10 μm) and is thus challenging to implement in studies of single relatively-short nanotubes. FCS has provided valuable information on diffusion rates and adsorption/desorption kinetics in studies of organic nanotubes.[18] Although it offers high temporal and spatial resolution, it is not well suited for imaging of the diffusion dynamics in heterogeneous materials. Such experiments would require that several long time transients be recorded sequentially at a number of different positions along each nanotube. Imaging-FCS is a multichannel variant of FCS that allows for many time transients to be collected simultaneously across a broad image area, greatly enhancing the data acquisition rate, albeit with some sacrifice in time resolution. Imaging-FCS has also been shown to afford sub-diffraction-limited spatial resolution.[19] Such experiments are usually performed using fast frame-rate electron-multiplying CCD (EM-CCD) cameras. Autocorrelation of the time transient obtained at each image pixel is then used to determine the time scale for diffusion.

In this paper, imaging-FCS was employed to investigate both the rate and mechanism of diffusion for sulforhodamine B (SRB) dye molecules doped into bolaamphiphile-based self-assembled organic nanotubes. The SRB dye served as a model for anionic molecules that might be loaded into and released from these nanotubes in drug delivery applications. The dye-doped nanotubes were dispersed on glass substrates so that individual nanotubes could be located and imaged one at a time, using wide-field fluorescence video microscopy. They were immersed in buffer solution to mobilize the dye molecules within the nanotubes. Wide-field video data acquired from isolated nanotubes were collected, autocorrelated on a pixel-by-pixel basis, and the autocorrelation decays fit to an appropriate model to determine the apparent diffusion coefficient of the dye as a function of position along each tube. Both the ionic strength and the pH of the buffer solution were varied as a means to modulate any coulombic interactions between the SRB molecules and the charged inner surfaces of the nanotubes. The results showed that SRB diffusion was governed by more than the random thermal motions of Fickian diffusion, with coulombic interactions playing an integral role in slowing mass transport of the dye. The results of this study will aid in the development of bolaamphiphile-based nanotubes for use in controlled drug release applications by providing a better understanding of the factors governing the rates and mechanisms of mass transport within the nanotubes.

Experimental considerations

Materials

An asymmetric bolaamphiphile, **1**, *N*-(β-D-glucopyranosyl)-*N*′-(2-glycylglycylglycine-amideethyl)-icosane-diamide was employed as the organic nanotube precursor.[21] Its structure is shown in Fig. 1a. Self-assembled cylindrical nanotubes of regular molecular packing were obtained from monomer **1** according to the following procedure: monomer **1** (10 mg) was refluxed in 18 MΩ cm water (10 mL) for 10 min, and then gradually cooled to room temperature. Subsequently, aqueous NaOH solution (0.1 M, 200 μL) was added to obtain a turbid solution containing organic nanotubes. The resultant nanotubes consist of a single layer of bolaamphiphiles, in which hydrogen bonds strongly hold the polyglycine-II-type network together.[21] The inner and outer surfaces of the nanotubes are terminated with ammonia and glucose headgroups, respectively (Fig. 1a).

The nanotubes were dispersed on glass coverslips for imaging experiments. In this process, aqueous nanotube solution (0.1 mg mL^{-1}) was drop cast on a plasma-cleaned glass coverslip, and the water was allowed to evaporate. The coverslip was subsequently rinsed with water to remove any loosely adsorbed nanotubes and blown dry with nitrogen. The nanotubes remaining on the surface were then doped with SRB (Acros Organics) for fluorescence imaging. The structure of SRB is shown in Fig. 1d. The nanotubes were dyed by depositing 200 μL of 120 μM SRB in aqueous solution over the coverslip. This solution was allowed to sit in contact with the nanotubes for a period of 2 h. The coverslip was then rinsed with 18 MΩ cm water and blown dry with nitrogen. This final rinsing step removed SRB molecules loosely bound to the exterior of the nanotubes and to the coverslip surface.[18]

Fluorescence videos of the nanotubes were acquired under buffer solution. To maintain contact between the buffer and nanotube samples, a rectangular polydimethylsiloxane (PDMS) well was fabricated and placed over the coverslip. The PDMS well was filled with any one of a series of phosphate buffered saline (PBS) solutions (Aldrich), immediately prior to the imaging experiments. The PDMS well was then covered with a PDMS slab to prevent solution evaporation. The PBS solutions employed were buffers of pH 6.4, 7.4 and 8.4. Each was prepared in four different ionic strengths (1.73 mM, 17.3 mM, 173 mM and 520 mM).

Fluorescence microscopy

Images of individual dye-doped nanotubes were acquired on an inverted epi-illumination microscope (Nikon TiE) that has been described previously in detail.[22] Briefly, light from an argon ion laser (514 nm) was used to excite SRB fluorescence. Total internal reflection fluorescence (TIRF) mode was employed to minimize background fluorescence from bulk solution. An oil immersion objective (Nikon Apo TIRF 100×, 1.49 numerical aperture) was used for sample illumination and for collection of the emitted fluorescence. The incident laser power was maintained at 0.8 mW in all experiments. This power level afforded a sufficient signal-to-noise ratio while also reducing photobleaching of the dye molecules. Fluorescence collected from the sample was directed through an appropriate dichroic mirror and bandpass filter (Chroma 580/40) to block residual source light. Fluorescence videos were acquired by detecting SRB fluorescence with an EM-CCD camera (Andor iXon DU-897). Videos were acquired with 2 ms exposure time, and ~6 ms cycle time.

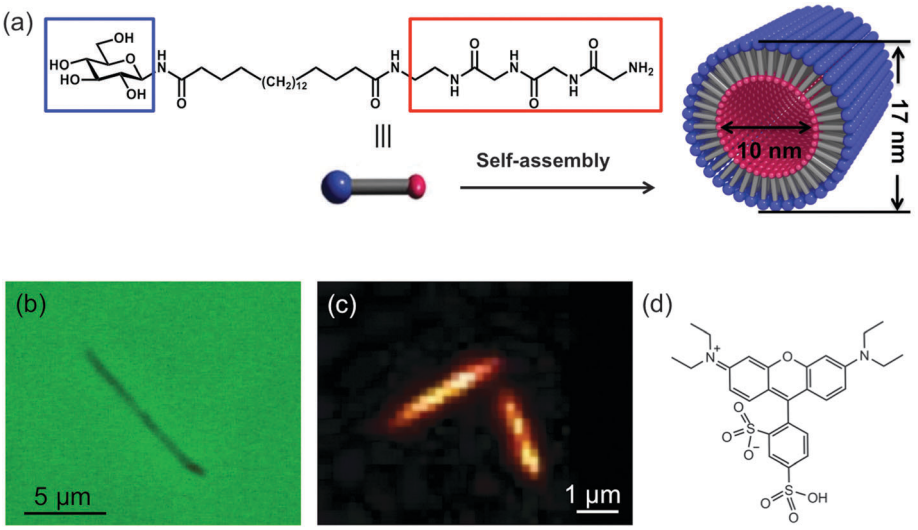

Fig. 1 (a) Bolaamphiphile monomer structure, **1**, and illustration of the molecular packing in the organic nanotubes. (b) Optical phase contrast image of one nanotube. (c) Wide-field fluorescence image of sulforhodamine B stained nanotubes. Different nanotubes are shown in panels b and c. (d) Structure of sulforhodamine B.

The EM gain was set to 30, the readout rate to 10 MHz, and 3 × 3 pixel binning was employed. Each video was 25 000 frames in length. The excitation region in the images covered a relatively large lateral area of 32 μm × 32 μm. Images were initially recorded from the full field of view to identify and locate individual nanotubes. Much smaller regions (~2.5 μm × 2.5 μm) showing individual nanotubes were then selected and video data acquired. The videos were subsequently loaded into a program written in the LabView (National Instruments) programming environment. This software subtracted the image background and calculated the temporal autocorrelation function at each pixel, across the final 20 000 video frames. The autocorrelation decays were subsequently fit to an appropriate model that included contributions from dye diffusion and photobleaching (see below).

Results & discussion

Wide-field fluorescence images

The nanotubes studied in this work are 10 nm in inner diameter, 3.5 nm in wall thickness and several micrometers in length.[21] Fig. 1b shows an optical phase contrast image obtained from one nanotube. While this tube appears to be slightly bent at one end, only straight nanotubes were selected for further investigation. Fig. 1c shows a wide-field fluorescence image obtained from a pair of SRB stained nanotubes. As with all fluorescence videos employed below, this image was acquired in TIRF mode in order to minimize background fluorescence from bulk solution. The nanotubes can be clearly distinguished above the background, owing to SRB staining. These tubes are ~2 μm in length, close to the average length of the full population of nanotubes examined in these studies. Videos were typically recorded of individual nanotubes.

Representative video data from a single nanotube is shown in Fig. 2a. This image was obtained by averaging the fluorescence across 20 000 video frames at each pixel. The original video is provided in ESI.† The apparent width of the nanotube shown is ~375 nm (full-width-at-half-maximum). Its width is much larger than the expected value of 17 nm because of the limited spatial resolution (~240 nm) of the optical imaging system. Neither the image shown in Fig. 2a, nor the original video data show clear evidence of fluorescent spots produced by individual SRB molecules. This is likely due to the presence of several dye molecules within the nanotube. Because of their brightness, the individual nanotubes can be clearly differentiated from much weaker fluorescent spots found in the surrounding regions. These background spots may reflect the presence of very short nanotubes, nanotube fragments, or residual unassociated SRB molecules.

The fluorescence intensity observed along a single nanotube can potentially provide information on the uniformity of nanotube doping. Indeed, the average fluorescence intensity

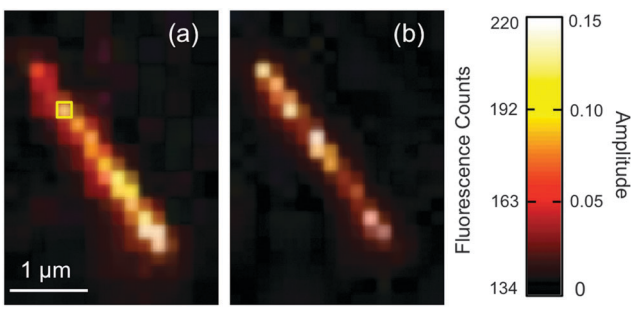

Fig. 2 (a) Representative wide-field fluorescence video data from an organic nanotube in PBS buffer solution at pH 7.4 and 1.73 mM ionic strength. The video is presented as an image and was obtained by averaging the fluorescence across 20 000 frames. (b) Image showing the fitted autocorrelation decay amplitude for each pixel in (a). Scale bars show the fluorescence counts (in 2 ms, left) and amplitude values (right) for panels (a) and (b), respectively.

(averaged across 20 000 video frames) was found to vary along the length of the nanotube shown in Fig. 2a. Such spatial variations in average fluorescence were observed in virtually every nanotube imaged in these studies. This observation suggests that the tubes were not uniformly doped with SRB. However, no clear trend in the position dependence of the signal levels could be identified, as discussed further in ESI.† It is believed the non-uniform fluorescence of the nanotubes may reflect the relatively low concentration (quasi single molecule levels) of dye found within the nanotubes. Furthermore, the fluorescence intensity of local regions along the individual tubes was observed to vary in time. These variations are consistent with time dependent variations in the local concentration of dye and are attributable to Brownian-like motion of the SRB molecules within the nanotubes.

Imaging fluorescence correlation spectroscopy

The apparent diffusion coefficients for SRB molecules diffusing within the nanotubes were determined by autocorrelating the fluorescence video data on a pixel-by-pixel basis and fitting the autocorrelation decays obtained to an appropriate model. Fig. 3a plots a representative time transient obtained from the pixel highlighted by the yellow box in Fig. 2a. The fluorescence spikes shown in the time transient depict signal fluctuations attributable to diffusion of individual SRB molecules in and out of the detection volume along the nanotube. It is the mean time scale of these signal fluctuations that gives a measure of the apparent diffusion coefficient for the SRB molecules. However, the signal level also gradually decays in time due to the inevitable photobleaching of the limited number of dye molecules found within the nanotube. The background fluorescence from regions surrounding the nanotube also exhibits a similar bleaching decay. It should be noted that no dye was added to the buffer solution and hence, the bleaching was essentially permanent.

Individual time transients were obtained from each pixel along the tube in each video. The time transient data were then autocorrelated as follows:

$$C(\tau) = \frac{\langle i(t)i(t+\tau)\rangle}{\langle i(t)\rangle^2} - 1 \qquad (1)$$

where $i(t)$ is the time transient data, $i(t+\tau)$ is the time transient shifted by a time lag, τ, and the brackets, $\langle\ \rangle$, indicate the time averaged value is calculated. Fig. 3b shows the autocorrelation function obtained from the time transient in Fig. 3a (red data points). While the autocorrelation function was obtained from the full 20 000 frames, it is only plotted out to τ = 1200 frames, due to the limited signal averaging that occurs at longer lag times.[23–25] The autocorrelation functions obtained from the nanotubes commonly incorporate two decay components: one attributable to mass transport of the SRB molecules and the other to SRB bleaching. As is readily apparent from the data shown in Fig. 3, fluctuations due to diffusion occur on a several second time scale, while the bleaching decay occurs over several tens of seconds. Because of the approximately 10-fold difference in these two time scales, the contributions of diffusion and bleaching can readily be distinguished.

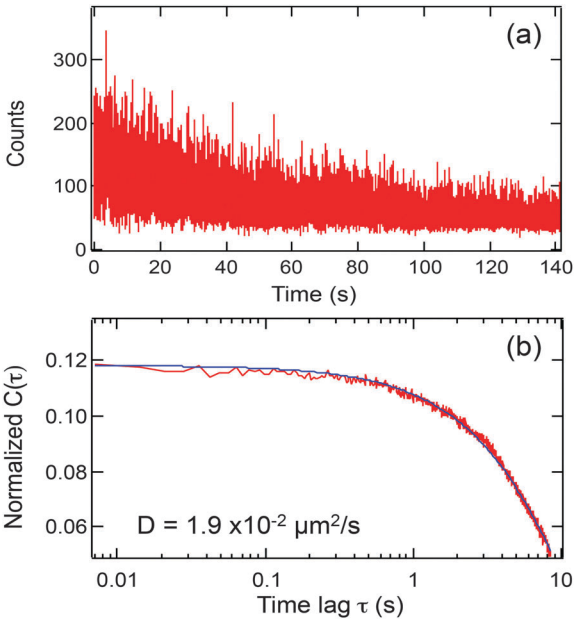

Fig. 3 (a) Representative time transient from the one pixel in Fig. 2a (yellow box); (b) autocorrelation function (red line) derived from the data in (a), using eqn (1) and its fit to eqn (2) (blue line).

In selecting an appropriate model for use in fitting of the autocorrelation functions, it was noted that the nanotube inner diameter ($\sim$10 nm)[21] is very small compared to its length ($>$2 μm). Therefore, SRB diffusion within the tube is expected to be strongly confined to 1D. Furthermore, no evidence of long adsorption events, such as have been observed previously for diffusion of charged dyes near other charged surfaces,[26,27] was found in any of the videos acquired in the present studies. The absence of anomalously long adsorption events suggests that a model for Fickian diffusion may be appropriate. The equation employed for fitting of the data thus included components for both 1D diffusion and photobleaching, and is given by:[28]

$$C(\tau) = \frac{A}{\sqrt{1+\frac{\tau D}{\sigma^2}}} \times \frac{(\exp[k(T-\tau)]-1)}{k(T-\tau)} \qquad (2)$$

Here, D represents the apparent diffusion coefficient of the SRB molecules within the tube, A is the amplitude of the autocorrelation decay, σ^2 is the squared radius of the detection region ($\sigma \sim$ 0.310 μm), k represents the bleaching decay rate constant, and T is the total length of the video in time. While all parameters could be obtained by fitting the individual autocorrelation decays, the bleaching time constant was instead obtained by separately fitting the decay of the background fluorescence in each video. The bleaching decay constant obtained was then employed in eqn (2) as a constant parameter, with the only adjustable parameters being A and D. The zero delay point (τ = 0) was not included in the fitting process as its value includes contributions from significant uncorrelated noise.

Fig. 2b shows the amplitude data obtained by fitting the autocorrelation function from each image pixel in Fig. 2a. Brighter pixels indicate larger amplitudes. The amplitude image

reveals the tube location and width with improved, sub-diffraction-limited spatial resolution,[19] which can be observed as a narrowing of the tube image between Fig. 2a and b.

Concentration dependence. The autocorrelation decay amplitude is often used as a means to estimate the concentration of diffusing molecules in a sample and is expected to be inversely dependent upon the concentration of diffusing dye molecules.[29] However, as noted in previous work,[30] a more complicated concentration dependence occurs in the presence of significant background. In this case, the autocorrelation amplitude actually increases with increasing dye concentration, passes through a maximum, and subsequently decreases. In order to fully understand the conditions under which the present data were acquired, autocorrelation results were obtained as a function of dye concentration in the nanotubes, which was varied by changing the SRB concentration in the loading solution from 10 μM to 70 mM. It was found that the autocorrelation amplitude initially rises with dye concentration, peaks at ~140 μM and later decreases, as expected.[30] The decrease in the autocorrelation amplitude at higher dye concentrations is consistent with assignment of the signal fluctuations to single molecule diffusion phenomena. Because of this rather complex concentration dependence, no conclusions on the uniformity of dye loading could be drawn from the autocorrelation amplitude data. However, these results were used instead to select an optimum dye concentration of 120 μM for loading of the nanotubes, as it provides relatively high amplitudes while avoiding the possibility for SRB dimerization.[31] All subsequent experiments were performed on nanotubes loaded at this concentration.

Apparent diffusion coefficients. The autocorrelation fits also provide valuable data on the apparent diffusion coefficient, D, at each image pixel along each nanotube (see eqn (2)). The D value obtained from the pixel highlighted in Fig. 2a is 1.9×10^{-2} μm^2 s^{-1}, based on the fit shown in Fig. 3b. The D values obtained along the full length of this same nanotube are similar and are best depicted as an image constructed from the D values. While an apparent D value is obtained from every image pixel, many of the pixels have little or no signal and so their D values are often meaningless. The former are found off the tube, over background regions, while the values obtained from the nanotube itself are useful. To better depict regions where meaningful D values were obtained, a composite 3D image was prepared, as shown in Fig. 4. This image depicts the autocorrelation amplitude as height and the measured D value by the image color. The amplitudes are very close to zero off the tube, where little or no dye diffusion is detected. Likewise, the D values obtained off the tube vary substantially from pixel to pixel because they are dominated by noise. In contrast, the D values obtained along the tube are largely invariant with position, as depicted by the uniform image color along the nanotube axis. This image suggests the D values are qualitatively similar along the tube length. Further analysis of the position dependence of D is provided in ESI,† along with data from two different nanotubes. These results demonstrate that similar D values were obtained from a number of nanotubes.

Averages of the data obtained along the full length of the aforementioned nanotubes (Fig. 4, Fig. S1a and b, ESI†) yield D values of 1.6×10^{-2} μm^2 s^{-1}, 5.6×10^{-2} μm^2 s^{-1} and 1.9×10^{-2} μm^2 s^{-1}, respectively. These values are all substantially smaller than the diffusion coefficient of SRB in bulk solution, which has been reported to be 470 μm^2 s^{-1}.[32] It is possible that coulombic interactions between the anionic dye molecules and the cationic inner surfaces of the nanotubes could lead to rapid, reversible adsorption of dye to these surfaces, slowing its apparent diffusive motions. The difference between the bulk and apparent nanotube D values could also be the result of an increase in the viscosity of the solution inside the nanotubes. The D values should then scale inversely with the local viscosity, as defined by the Stokes–Einstein relation. However, the 10^4-fold reduction in D is too large to be explained by an increase in the viscosity of the water filling the nanotubes. Alternatively, the organic phase of the nanotube walls may provide the high viscosity environment suggested by the small D values. In this case, the SRB molecules would need to partition from the aqueous phase into the walls of the nanotubes. This possibility may be discounted because the octanol–water partition coefficient (K_{ow}) for SRB is ~0.0095,[33] indicating that the dye is very polar and most likely confined to the aqueous phase inside the nanotubes. While it has been demonstrated that water confined within organic nanotubes having glucose moieties on their inner surfaces exhibits a 20% decrease in polarity compared to bulk water,[34] this effect is deemed insufficient to dramatically enhance partitioning of the SRB into the nanotube walls. As with many organic dyes, SRB may aggregate in aqueous solution, altering its physical size and reducing its rate of diffusion. While SRB dimers have been reported to form at cationic surfaces,[35] such species would be immobilized inside the nanotubes and would not contribute to the measured D values. SRB aggregates in aqueous solution have only been found under relatively extreme (*i.e.* high salt content) conditions that are far different from those of the present experiments.[31] It is concluded that coulombic interactions between the dye and

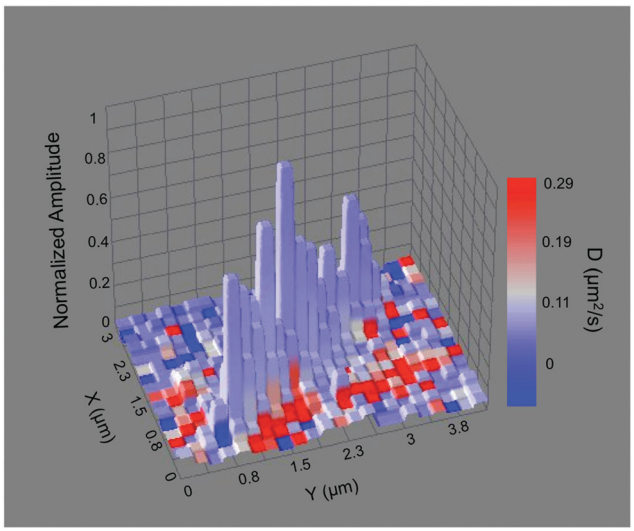

Fig. 4 3D surface plot showing a composite image of the nanotube in Fig. 2 with the normalized autocorrelation amplitude shown as height, and the measured diffusion coefficient depicted by the color scale.

nanotube inner surface are the most likely cause of slow SRB diffusion.

It should be noted that SRB diffusion is also slower than might be expected from prior literature results. For example, the diffusion of green fluorescent protein (GFP) has previously been investigated inside similar organic nanotubes by FRET methods.[36] In this case, the average diffusion coefficient was found to be 0.36 $\mu m^2 s^{-1}$ at pH 6.8, approximately 7-fold larger than the D values measured for SRB. This apparent discrepancy may reflect differences in experimental details: GFP is surrounded by stabilizing agents such as glycerol (20 wt%), and thus its interactions with the cationic sites on the nanotube inner surface are suppressed, while SRB is expected to interact more strongly with the nanotube. The possible role played by coulombic interactions in limiting SRB diffusion is the focus of the remainder of this report.

Ionic strength dependence of SRB diffusion

The role played by coulombic interactions in governing mass transport of the SRB molecules can be explored by altering the ionic strength of the aqueous solution filling the nanotubes. Higher ionic strengths will lead to narrower electrical double layers (*i.e.* shorter Debye lengths) at the nanotube surfaces. These conditions will better screen any coulombic interactions between the anionic dye and cationic sites on the nanotube surfaces, and are expected to lead to an increase in the apparent rate of SRB diffusion.

The average SRB diffusion coefficients obtained from several different nanotubes are plotted as a function of Debye length in Fig. 5a. These data were acquired by averaging across the entire length of each tube and then averaging the individual tube data. The data shown are for ionic strengths of 1.73 mM, 17.3 mM, 173 mM and 520 mM, at three different pH values. The pH dependence of the data is discussed below. In all cases, the diffusion coefficients showed similar trends, with D increasing as the Debye length decreased from 7.4 nm to 0.74 nm (*i.e.*, with increasing ionic strength). The D values subsequently decreased as the Debye length decreased to 0.4 nm. It is noteworthy that the electric double layers from opposite surfaces inside the nanotubes overlap when the Debye length is as large as 7.4 nm. Under this condition, relatively little screening of the dye and nanotube surface charges occurs and relatively strong dye-surface interactions are expected. As the ionic strength increases and the Debye length becomes shorter, the apparent SRB diffusion coefficient initially increases, consistent with increased coulombic screening. The decrease in the apparent SRB diffusion coefficient at the highest ionic strength is suggestive of a change in the nature of the physical interactions governing SRB motion. This latter observation might be explained by a "salting out" of SRB at the highest ionic strength, leading to an abrupt increase in the strength of the relevant dye-surface interactions.

pH dependence of SRB diffusion

While the dependence of the apparent SRB diffusion coefficient on solution ionic strength is consistent with a slowing of dye motion caused by coulombic interactions between the dye and

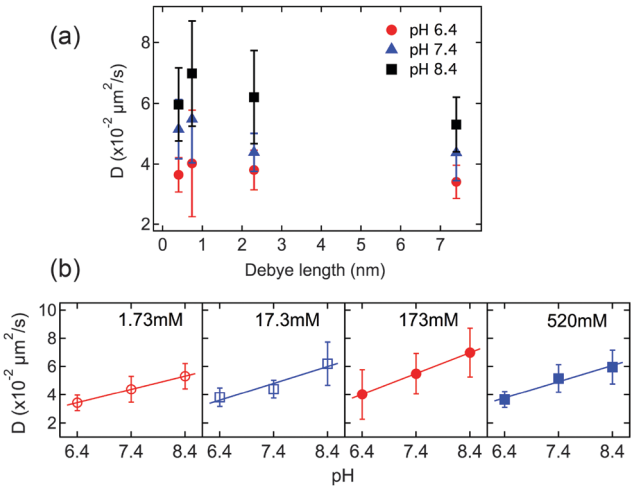

Fig. 5 Average apparent diffusion coefficients for SRB as a function of Debye length (a) and buffer pH (b). Error bars are standard errors on the mean. The solid lines fitted to the data in (b) have been added only as a means to better depict the trends in the data.

nanotube surface, it does not necessarily confirm a dependence on surface charge. Such a dependence is best demonstrated by monitoring SRB diffusion under different surface charge conditions. The surface charge was readily altered by changing the pH of the buffer solution filling the nanotubes. The pK_a of the ammonium groups on similar nanotubes (having the same headgroups but thinner hydrophobic walls) has been determined to be 7.27.[11] As the solution pH increases above 7.27, the density of ammonium ions on the inner nanotube surface will decrease, while lower pH values will lead to an increase in surface charge density. In the present studies, buffers having pH values of 6.4, 7.4 and 8.4 were employed to explore a range of surface charge conditions. It is noteworthy that the pK_a of the highly acidic sulfonic groups on the SRB dye is <1.5.[33] Therefore, the SRB molecules will remain negatively charged across the range of pH values investigated.

Fig. 5b plots the average apparent SRB diffusion coefficients as a function of pH for the four different ionic strengths. The numerical values used in construction of Fig. 5 are given in Table 1. Each set of data reveals a clear trend towards higher D with increasing buffer pH. At pH 6.4, the amine groups on the inner nanotube surfaces should be almost fully ($\sim$90%) protonated, while at pH 7.4 and 8.4, the expected degree of protonation decreases substantially ($\sim$43% and $\sim$7%, respectively).[11] The results in Fig. 5b therefore demonstrate a clear surface charge dependence in the apparent D values, consistent with an important role for coulombic interactions in governing mass transport.

It should be noted that the simple calculations presented above suggest that the surface charge density varies by more than an order of magnitude for the range of solution pH values investigated, while the observed D values change by only a factor of two. This apparent discrepancy has several possible origins. First, coulombic interactions may represent only one of several phenomena leading to slow dye diffusion, with pH independent phenomena also playing a role. For example,

Table 1 Summary of the mean apparent diffusion coefficients ($\times 10^{-2}$ μm^2 s^{-1}) with standard errors on the mean at each solution pH and ionic strength investigated. The number of nanotubes characterized in each case is given in parentheses

	pH 6.4	pH 7.4	pH 8.4
1.73 mM	3.4 ± 0.6 (11)	4.4 ± 0.9 (9)	5.3 ± 0.9 (6)
17.3 mM	3.8 ± 0.7 (7)	4.4 ± 0.6 (12)	6.2 ± 1.5 (10)
173 mM	4.0 ± 1.8 (7)	5.5 ± 1.5 (10)	7.0 ± 1.7 (5)
520 mM	3.7 ± 0.6 (10)	5.2 ± 1.0 (10)	6.0 ± 1.2 (17)

an increase in solution viscosity inside the nanotubes could also contribute to the slowing of SRB diffusion. Second, coulombic interactions between the surface and dye might become saturated above a certain surface charge density. The density of amine groups on the nanotube surface is estimated to be $\sim 4 \times 10^{14}$ cm^{-2}, suggesting a distance of ~ 0.5 nm between cationic sites at pH = 6.4. At pH = 8.4, the distance between cationic sites is ~ 1.9 nm, a factor of only ~ 4 greater. As the energy of coulombic interactions scales linearly with distance, this observation is consistent with a much smaller decrease in the role played by these interactions at higher pH. Third, it is well known from the literature on the acid–base chemistry of amine-modified surfaces that the pK_a of surface-bound ammonium ions decreases with increasing charge density.[37,38] Therefore, a significant fraction of amine groups cannot be protonated, even at very low pH. The charge density at pH = 6.4 is likely to be far smaller than predicted above, as a result.

Model for SRB mass transport in bolaamphiphile nanotubes

The results discussed above suggest a model for diffusion of negatively charged SRB molecules within the organic nanotubes. Fig. 6 provides a pictorial representation of this model in which the blue circles represent individual SRB molecules. Diffusion within the tubes clearly does not occur by a Fickian mechanism alone. The results above show a dependence on both the ionic strength and the pH of the aqueous buffer filling the nanotubes, and no such dependence is expected for Fickian diffusion. It is concluded that coulombic interactions between the SRB molecules and the inner nanotube surfaces play an important role in limiting mass transport of the dye. These interactions likely involve adsorption and desorption of the dye from the nanotube surface. Previous investigations of diffusion by charged dyes in close proximity to charged surfaces have demonstrated that the dyes can adsorb to the surface for long periods of time.[26,27] Such events appear as anomalously long upward fluctuations in the fluorescence signal from the detection volume. No evidence of such long adsorption events was found in any of the videos obtained for these studies. It is thus concluded that adsorption of the anionic dye to the (possibly) positively charged inner surfaces of the nanotubes occurs at high frequency, and that these events are short-lived on the imaging time scale. These adsorption events retard or briefly interrupt dye motion, while dye diffusion most likely occurs within the aqueous solution filling the tubes once they desorb. Little or no contribution from SRB molecules that have partitioned into the tube walls is expected, because the dye partitions too strongly into the aqueous phase. In this case, the mechanism for mass transport of the anionic SRB molecules within the tubes may best be described as desorption-mediated Fickian diffusion, in which the dye molecules may be viewed as "hopping" between adsorption sites along the nanotube surface.

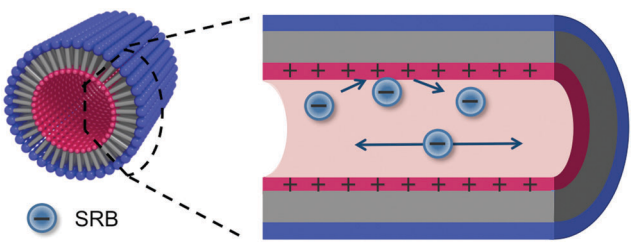

Fig. 6 Model for SRB diffusion inside the organic nanotubes. The blue circles carrying negative charges represent individual SRB molecules. Diffusion involves a fast "hopping" of the anionic molecules between cationic sites on the inner nanotube surface. The molecules are not drawn to scale to allow for better visualization.

Desorption-mediated diffusion has been observed for a wide variety of other materials as well.[39–41] Previous studies primarily employed single molecule tracking as a means to determine the mass transport mechanism and the dominance of desorption-mediated diffusion was revealed by a characteristic change in the single molecule step size distribution. In the present studies, we show that changes in the apparent rate of diffusion brought about by modulation of the dye-surface interactions can also be detected in imaging-FCS studies and used to identify contributions from non-Fickian mass transport mechanisms. The participation of desorption-mediated diffusion would otherwise be difficult to detect within short nanotubes because of the small distances over which molecular motions occur.

Conclusion

The rate and mechanism of diffusion for anionic SRB dye molecules within self-assembled organic nanotubes were investigated by imaging-FCS. The organic nanotubes were assembled from unique bolaamphiphile monomers and carry a pH-dependent positive charge on their inner surfaces. Related nanotubes are being investigated by others as vehicles for use in controlled drug delivery.[6–8] The imaging-FCS data revealed that the SRB molecules moved along the nanotube long axis and that their apparent rate of diffusion was dependent upon both the ionic strength and pH of the aqueous buffer filling the tubes. The apparent rate of SRB diffusion was found to increase with increasing solution ionic strength at relatively low buffer concentrations and then to decrease at the highest ionic strengths. The role played by surface charge was revealed through an observed increase in the apparent rate of SRB diffusion with increasing buffer pH. These observations demonstrated that coulombic interactions between the cationic ammonium ions on the nanotube inner surface and the anionic SRB molecules played an integral role in governing SRB diffusion. It was concluded that mass transport of the dye within the nanotubes

occurred by a desorption-mediated Fickian diffusion mechanism in which the dye molecules frequently adsorb to the nanotube inner surface and diffuse by Brownian-like motion when released from the surface into the solution filling the tube. While this work explores interactions between anionic dyes and the inner nanotube surface, studies of nanotube interactions with uncharged and cationic dyes are now underway and will be reported shortly.

The results of these studies provide a better understanding of mass transport phenomena relevant to the use of these and other organic nanotubes in drug delivery applications. They reveal how ionic strength and pH may be used to control the rate of mass transport of drug molecules within the nanotubes and suggest possible means to trigger their release. Enhanced knowledge of these phenomena promises to lead to improved performance of these materials in drug delivery applications.

Acknowledgements

The authors acknowledge support from the Division of Chemical Sciences, Geosciences, and Biosciences, Office of Basic Energy Sciences of the U.S. Department of Energy (DE-FG02-12ER16095).

References

1 T. Shimizu, M. Masuda and H. Minamikawa, Supramolecular Nanotube Architectures Based on Amphiphilic Molecules, *Chem. Rev.*, 2005, **105**, 1401–1443.
2 D. T. Bong, T. D. Clark, J. R. Granja and M. R. Ghadiri, Self-Assembling Organic Nanotubes, *Angew. Chem., Int. Ed.*, 2001, **40**, 988–1011.
3 T. Shimizu, H. Minamikawa, M. Kogiso, M. Aoyagi, N. Kameta, W. Ding and M. Masuda, Self-Organized Nanotube Materials and Their Application in Bioengineering, *Polym. J.*, 2014, **46**, 831–858.
4 T. Shimizu, Self-Assembled Organic Nanotubes: Toward Attoliter Chemistry, *J. Polym. Sci., Part A: Polym. Chem.*, 2008, **46**, 2601–2611.
5 N. Kameta, M. Masuda, H. Minamikawa, N. V. Goutev, J. A. Rim, J. H. Jung and T. Shimizu, Selective Construction of Supramolecular Nanotube Hosts with Cationic Inner Surfaces, *Adv. Mater.*, 2005, **17**, 2732–2736.
6 W. Ding, M. Wada, N. Kameta, H. Minamikawa, T. Shimizu and M. Masuda, Functionalized Organic Nanotubes as Tubular Nonviral Gene Transfer Vector, *J. Controlled Release*, 2011, **156**, 70–75.
7 X. Yan, Q. He, K. Wang, L. Duan, Y. Cui and J. Li, Transition of Cationic Dipeptide Nanotubes into Vesicles and Oligonucleotide Delivery, *Angew. Chem., Int. Ed.*, 2007, **46**, 2431–2434.
8 G. A. Hughes, Nanostructure-Mediated Drug Delivery, *Nanomedicine*, 2005, **1**, 22–30.
9 N. Kameta, M. Masuda, H. Minamikawa, Y. Mishima, I. Yamashita and T. Shimizu, Functionalizable Organic Nanochannels Based on Lipid Nanotubes: Encapsulation and Nanofluidic Behavior of Biomacromolecules, *Chem. Mater.*, 2007, **19**, 3553–3560.
10 R. Langer, Drug Delivery and Targeting, *Nature*, 1998, **392**, 5–10.
11 N. Kameta, H. Minamikawa, M. Masuda, G. Mizuno and T. Shimizu, Controllable Biomolecule Release from Self-Assembled Organic Nanotubes with Asymmetric Surfaces: pH and Temperature Dependence, *Soft Matter*, 2008, **4**, 1681–1687.
12 Y. Fu and W. J. Kao, Drug Release Kinetics and Transport Mechanisms of Non-Degradable and Degradable Polymeric Delivery Systems, *Expert Opin. Drug Delivery*, 2010, **7**, 429–444.
13 C. Maderuelo, A. Zarzuelo and J. M. Lanao, Critical Factors in the Research of Drugs from Sustained Release Hydrophilic Matrices, *J. Controlled Release*, 2011, **154**, 2–19.
14 D. A. Higgins, S. C. Park, K.-H. Tran-Ba and T. Ito, Single-Molecule Investigations of Morphology and Mass Transport Dynamics in Nanostructured Materials, *Annu. Rev. Anal. Chem.*, 2015, **8**, 193–216.
15 D. A. Higgins, K.-H. Tran-Ba and T. Ito, Following Single Molecules to a Better Understanding of Self-Assembled One-Dimensional Nanostructures, *J. Phys. Chem. Lett.*, 2013, **4**, 3095–3103.
16 K.-H. Tran-Ba, D. A. Higgins and T. Ito, Fluorescence Recovery after Photobleaching and Single-Molecule Tracking Measurements of Anisotropic Diffusion within Identical Regions of a Cylinder-Forming Diblock Copolymer Film, *Anal. Chem.*, 2015, **87**, 5802–5809.
17 K. Okamoto, C. J. Shook, L. Bivona, S. B. Lee and D. S. English, Direct Observation of Wetting and Diffusion in the Hydrophobic Interior of Silica Nanotubes, *Nano Lett.*, 2004, **4**, 233–239.
18 L. Guo, P. Chowdhury, J. Fang and F. Gai, Heterogeneous and Anomalous Diffusion Inside Lipid Tubules, *J. Phys. Chem. B*, 2007, **111**, 14244–14249.
19 L. Kisley, R. Brunetti, L. J. Tauzin, B. Shuang, X. Yi, A. W. Kirkeminde, D. A. Higgins, S. Weiss and C. F. Landes, Characterization of Porous Materials by Fluorescence Correlation Spectroscopy Super-resolution Optical Fluctuation Imaging, *ACS Nano*, 2015, **9**, 9158–9166.
20 A. W. Kirkeminde, T. Torres, T. Ito and D. A. Higgins, Multiple Diffusion Pathways in Pluronic F127 Mesophases Revealed by Single Molecule Tracking and Fluorescence Correlation Spectroscopy, *J. Phys. Chem. B*, 2011, **115**, 12736–12743.
21 N. Kameta, S. J. Lee, M. Masuda and T. Shimizu, Biologically Responsive, Sustainable Release from Metallo-Drug Coordinated 1D Nanostructures, *J. Mater. Chem. B*, 2013, **1**, 276–283.
22 K. H. Tran Ba, T. A. Everett, T. Ito and D. A. Higgins, Trajectory Angle Determination in One Dimensional Single Molecule Tracking Data by Orthogonal Regression Analysis, *Phys. Chem. Chem. Phys.*, 2011, **13**, 1827–1835.
23 D. E. Koppel, Statistical Accuracy in Fluorescence Correlation Spectroscopy, *Phys. Rev. A: At., Mol., Opt. Phys.*, 1974, **10**, 1938–1945.
24 A. Tcherniak, C. Reznik, S. Link and C. F. Landes, Fluorescence Correlation Spectroscopy: Criteria for Analysis in Complex Systems, *Anal. Chem.*, 2009, **81**, 746–754.

25 G. K. Schenter, H. P. Lu and X. S. Xie, Statistical Analyses and Theoretical Models of Single-Molecule Enzymatic Dynamics, *J. Phys. Chem. A*, 1999, **103**, 10477–10488.
26 M. J. Wirth and D. J. Swinton, Single-Molecule Probing of Mixed-Mode Adsorption at a Chromatographic Interface, *Anal. Chem.*, 1998, **70**, 5264–5271.
27 Y. Fu, F. Ye, W. G. Sanders, M. M. Collinson and D. A. Higgins, Single Molecule Spectroscopy Studies of Diffusion in Mesoporous Silica Thin Films, *J. Phys. Chem. B*, 2006, **110**, 9164–9170.
28 D. L. Kolin, S. Costantino and P. W. Wiseman, Sampling Effects, Noise, and Photobleaching in Temporal Image Correlation Spectroscopy, *Biophys. J.*, 2006, **90**, 628–639.
29 E. L. Elson and D. Magde, Fluorescence Correlation Spectroscopy. I. Conceptual Basis and Theory, *Biopolymers*, 1974, **13**, 1–27.
30 F. Ye, M. M. Collinson and D. A. Higgins, Molecular Orientation and Its Influence on Autocorrelation Amplitudes in Single-Molecule Imaging Experiments, *Anal. Chem.*, 2007, **79**, 6465–6472.
31 R. W. Chambers, T. Kajiwara and D. R. Kearns, Effect of Dimer Formation on the Electronic Absorption and Emission Spectra of Ionic Dyes. Rhodamines and Other Common Dyes, *J. Phys. Chem.*, 1974, **78**, 380–387.
32 D. A. Sabatini, Sorption and Intraparticle Diffusion of Fluorescent Dyes with Consolidated Aquifer Media, *Groundwater*, 2000, **38**, 651–656.
33 T. Kasnavia, D. Vu and D. A. Sabatini, Fluorescent Dye and Media Properties Affecting Sorption and Tracer Selection, *Groundwater*, 1999, **37**, 376–381.
34 H. Yui, Y. Guo, K. Koyama, T. Sawada, G. John, B. Yang, M. Masuda and T. Shimizu, Local Environment and Property of Water Inside the Hollow Cylinder of a Lipid Nanotube, *Langmuir*, 2005, **21**, 721–727.
35 K. Ray and H. Nakahara, Adsorption of Sulforhodamine Dyes in Cationic Langmuir–Blodgett Films: Spectroscopic and Structural Studies, *J. Phys. Chem. B*, 2002, **106**, 92–100.
36 N. Kameta, H. Minamikawa, Y. Someya, H. Yui, M. Masuda and T. Shimizu, Confinement Effect of Organic Nanotubes Toward Green Fluorescent Protein (GFP) Depending on the Inner Diameter Size, *Chem. – Eur. J.*, 2010, **16**, 4217–4223.
37 E. W. van der Vegte and G. Hadziioannou, Acid-Base Properties and the Chemical Imaging of Surface-Bound Functional Groups Studied with Scanning Force Microscopy, *J. Phys. Chem. B*, 1997, **101**, 9563–9569.
38 P. R. Moses, L. M. Wier, J. C. Lennox, H. O. Finklea, J. R. Lenhard and R. W. Murray, X-ray Photoelectron Spectroscopy of Alkylaminesilanes Bound to Metal Oxide Electrodes, *Anal. Chem.*, 1978, **50**, 576–585.
39 M. J. Skaug, J. N. Mabry and D. K. Schwartz, Single-Molecule Tracking of Polymer Surface Diffusion, *J. Am. Chem. Soc.*, 2014, **136**, 1327–1332.
40 R. Walder, N. Nelson and D. K. Schwartz, Single Molecule Observations of Desorption-Mediated Diffusion at the Solid-Liquid Interface, *Phys. Rev. Lett.*, 2011, **107**, 156102.
41 D. Giri, K. M. Ashraf, M. M. Collinson and D. A. Higgins, Single-Molecule Perspective on Mass Transport in Condensed Water Layers over Gradient Self-Assembled Monolayers, *J. Phys. Chem. C*, 2015, **119**, 9418–9428.